# Synthesis, Biological Evaluation and Molecular Modeling Studies of Chiral Chloroquine Analogues as Antimalarial Agents

Srinivasarao Kondaparla[a†], Utsab Debnath[a†], Awakash Soni[b], Vasantha Rao Dola[a], Manish Sinha[a], Kumkum Srivastava[b], Sunil K. Puri[b] and Seturam B. Katti[*a]

[a]*Medicinal and Process Chemistry Division, CSIR-Central Drug Research Institute, Lucknow 226031, India*

[b]*Parasitology Division, CSIR-Central Drug Research Institute, Sector-10, Jankipuram Extension, Sitapur Road, Lucknow-226031, India*

[†] *These two authors contributed equally to this work*

**Abstract:** In a focused exploration, we have designed synthesized and biologically evaluated chiral conjugated new chloroquine (CQ) analogues with substituted piperazines as antimalarial agents. *In vitro* as well as *in vivo* studies revealed that compound **7c** showed potent activity [for *in vitro* $IC_{50}$= 56.98nM (3D7), 97.76nM (K1); for *in vivo* (up to at the dose of 12.5 mg/kg); SI = 3510] as a new lead of antimalarial agent. Other compounds **6b**, **6d**, **7d**, **7h**, **8c**, **8d**, **9a** and **9c** are also showing moderate activity against CQ-sensitive (3D7) strain and superior activity against resistant (K1) strain of *P. falciparum*. Furthermore, we have carried out docking and 3D-QSAR studies of all in-house data sets (168 molecules) of chiral CQ analogues to explain the structure activity relationships (SAR). Our new findings specified the significance of H-bond interaction with the side chain of heme for biological activity. In addition, the 3D-QSAR study against 3D7 strain indicated the favourable and unfavourable sites of CQ analogues for incorporating steric, hydrophobic and electropositive groups to improve the antimalarial activity.

**Key-words:** Piperazines, CQ-sensitive strain-3D7, Heme binding assay, *In-vitro* & *in-vivo* assay, Docking, 3D-QSAR.

**Corresponding author:** Tel: +91-522-2772454, Fax; +91-522-2771941 Email address: setu_katti@yahoo.com, (S. B. Katti)

## 1. Introduction

Malaria is a parasitic disease with high mortality and morbidity which sternly influence the socio-economic development of affected countries. [1]. It is one of the most prevalent parasitic disease, affecting nearly 300 million people around the globe annually [2]. Five species of *Plasmodium* (*P. falciparum*, *vivax*, *ovale*, *malariae and knowlesi*) are known to infect humans and *P. falciparum* causes the most severe form of infection. In erythrocytic stage, malaria parasite utilizes host haemoglobin for its growth and proliferation and convert toxic heme into non-toxic insoluble crystalline form called hemozoin [3]. However, in the infected erythrocytes, the mechanism of the conversion of heme to hemozoin through biochemical factors is not fully understood [4]. The inhibition of heme to hemozoin conversion in parasite is one of the most effective ways to treat malaria. Among the antimalarial agents quinoline scaffold have immense significance as forming a complex with heme in its monomer and μ-oxo dimer forms. Also, one of the 4-aminoquinoline based derivatives (Chloroquine; CQ) is most widely used for malaria treatment. [5-6]. Nevertheless, the widespread resistance of *P. falciparum* to CQ and artemisinin class of antimalarials has hampered the efforts to combat this deadly disease [7-8]. The resistance is a consequence of decreased accumulation of the drug in the food vacuole of the parasite owing to enhanced efflux and reduced uptake [9]. Therefore, it is an urgent need to modify the structure of CQ for the development of alternative drug like molecules that can circumvent the problem of *P. falciparum* resistance.

The SAR studies on CQ analogues revealed that compounds having shorter chain length are found to be active against CQ-resistant parasite strains [9-11]. By considering this scenario a number of research groups have synthesized new short chain analogues of 4-aminoquinolines, which were found considerably more potent than CQ against the resistant strain of *P. falciparum in vitro* [12]. However, Roepe *et al.* recently concluded that these observations only hold good for quinoline derivatives that contain a diethyl substituent on the terminal nitrogen [13]. It is believed that *N*-dealkylation reduces lipid solubility of these drugs and their derivatives leading to reduced antiplasomdial activity facilitating drug resistance [14]. Towards this objective, present researchers are putting efforts to modify the existing chemical moieties to get new leads for antimalarial activity. Previously from our group, we have investigated 4-aminoquinolines, synthesized by modulating the lipophilicity and basicity of lateral side chain attached to the 4-amino group of the CQ side chain [15-21]. Many of these analogues were found to form a complex with hematin and inhibit the *β*-

hematin formation, suggesting that this class of compounds act on a heme dimerization target. Also, many of these analogues have shown significant activity against CQ-resistant parasites.

Encouraged by these findings, we thought that fine-tuning of the terminal side chain with *N*-methylpiperazine could modulate the antimalarial activity [22]. Furthermore, from our laboratory several chiral chloroquine and its analogues were developed which showed excellent *in vitro* activity as compared to CQ [23]. As a part of our antimalarial drug discovery programme, the above mentioned results offered an ideal opportunity for better designing of molecules with chirally defined architecture and tailored pendant groups. Therefore, we have designed target specific compounds through a rational method. This rational method was used with special emphasis on avoiding metabolic *N*-dealkylation by incorporating bulkier substituents at adjacent part of the side chain and was evaluated for their antimalarial activity.

It has been seen that majority of analogues were found to have excellent activities against CQ-sensitive parasite strain 3D7. Nevertheless, no 3D-QSAR study has been reported earlier with this in-house data set of compounds. Therefore, we have focused on 3D-QSAR study of all in-house chiral chain based CQ analogues to explain the biological activity against 3D7 strain. Hence, in the present work we have developed our new findings through docking and 3D-QSAR study to get an insight about the importance of chiral chains in CQ analogues. Presence of H-bond interactions with heme in conjunction with favourable steric, hydrophobic and electropositive groups pave a novel way to design more potential analogues having anti-malarial activity against the CQ-resistant parasite strain.

## 2. Materials & Methods

### 2.1 Synthesis

**Synthesis of compounds (6a-6d, 7a-7h, 8a-8d, 9a-9d, 10a, 10b, 11a-11c and 12a)**

Synthesis of **6a-6d**, **7a-7h**, **8a-8d**, **9a-9d**, **10a**, **10b**, **11a-11c** and **12a** involves following steps starting from the preparation of the *Boc*-amino acids (**Figure 1**). Compounds **1a-1g** was converted to corresponding Boc derivatives **2a-2g** in quantitative yields. The *Boc* protected amino acids were converted to the corresponding methyl esters by using $K_2CO_3$/MeI in DMF solvent. Further, these esters were reduced to alcohols using sodium borohydride [24]. Boc amino alcohols were subjected to mesylation to afford **5a-5g** in good yields. The mesylated products were treated with *N*-substituted piperazines under nitrogen atmosphere in acetonitrile to get the desired compounds in good yields. Further, Boc

deprotection was accomplished using 20% HCl/Dioxane at room temperature in quantitative yields as corresponding hydrochloride salt. Hydrochloride salts were converted to free bases using triethylamine. Finally the intermediates (**6AD-6DD, 7AD-7CD, 7ED-7GD, 8AD-8DD, 9AD-9DD, 10AD-10BD, 11AD-11CD** and **12AD**) obtained were fused to 4,7-dichloroquinoline and/or 4-chloro-7-(trifluoromethyl)quinoline in the presence of phenol to obtain the title compounds [25]. All compounds were purified by the silica gel column chromatography and characterized by mass spectrometry, HRMS, $^{1}$H-NMR and $^{13}$C-NMR spectroscopy.

**2.2 Biological Methods**

**2.2.1. *In vitro* antiplasmodial assay**

The compounds were evaluated for antiplasmodial activity against 3D7 (CQ- sensitive) and K1 (CQ-resistant) strains of *Plasmodium falciparum* using Malaria SYBR Green I nucleic acid staining dye based fluorescence (MSF) assay as mentioned by Kondaparla *et al.* [26]. The stock (10 mM) solution was prepared in DMSO and test dilutions were prepared in culture medium (RPMI-1640-FBS). Chloroquine-diphosphate was used as reference drug. For assessment of antimalarial activity 50µl of culture medium was dispensed in 96 well plate followed by addition of 50 µL of highest concentration (< 0.5% of DMSO) of test compounds (in duplicate wells) in row B. Subsequently two-fold serial dilutions were prepared in culture medium and finally 50 µL of 2.0 % parasitized cell suspension containing 0.8 % parasitaemia (Asynchronous culture containing more than 80% ring stages) was added to each well except 4 wells in row 'A' received non parasitized erythrocyte suspension. The plates were incubated at 37 °C in $CO_2$ incubator in an atmosphere of 5% $CO_2$ and air mixture for 72 h. After 72 h 100 µL of lysis buffer containing 2x concentration of SYBR Green-I (Invitrogen) was added to each well and incubated for one hour at 37°C. The plates were examined at 485±20 nm of excitation and 530±20 nm of emission for relative fluorescence units (RFUs) per well using the fluorescence plate reader (FLX800, BIOTEK). Data was transferred into a graphic programme (EXCEL) and $IC_{50}$ values were obtained by Logit regression analysis of dose response curves using pre-programmed Excel spreadsheet. Three replicates were carried out for each compound.

**2.2.2 Determination of hematin 4-aminoquinoline derivatives association constant.**

Association constant for hematin and 4-aminoquinoline derivative complex formation were determined by spectrometric titration procedure in aqueous DMSO at pH-7.5[27]. In this

assay condition, hematin is strictly in monomeric state and interpretation of the results is not complicated by the need to consider hematin disaggregation process. Association constant calculated in this technique is a good refection of the interaction that would occur in the acidic food vacuole of the parasite and pH-7.5 improves the stability of hematin solutions and quality of the data.

**2.2.3. *In vitro* inhibition of *β*-hematin formation assay**

The ability of the 4-aminoquinoline derivatives to inhibit *β*-hematin formation was induced by 1-oleoyl-rac-glycerol. Spectroscopic measurements were done using UV spectrophotometer at 405 nm $\lambda_{max}$ and at pH 5 [28]. The $IC_{50}$ values obtained from the assay are expressed as percent inhibition relative to *β*-hematin formation in a drug free control. The $IC_{50}$ for the compounds were obtained from the sigmoidal dose-response curves using non-linear regression curve fitting analyses with GraphPad Prism v.3.00 software [29].

**2.2.4. *In vitro* assay for evaluation of cytotoxic activity**

Cytotoxicity of the compounds was carried out using Vero cell line (C1008; Monkey kidney fibroblast) following the method as mentioned in Sinha *et al.* [23]. The cells were incubated with compound-dilutions for 72 h and MTT was used as reagent for detection of cytotoxicity, 50% cytotoxic concentration ($CC_{50}$) was determined using the nonlinear regression analysis of dose response curves using the pre-programmed Excel spreadsheet. Selectivity index (SI) was calculated as:

$$SI = CC_{50} / IC_{50}$$

**2.2.5. *In vivo* antimalarial assay**

The *in vivo* drug response was evaluated in Swiss mice infected with *P. yoelii* (N-67 strain) which is innately resistant to CQ [30]. The mice (22±2 g) were inoculated with $1x10^6$ parasitized RBC on day 0 and treatment was administered to a group of five mice from day 0-3, once daily. The aqueous suspensions of compounds were prepared with a few drops of Tween 80. The efficacy of test compounds was evaluated at 100 mg/kg/day and the required daily dose was administered in 0.5 mL volume via oral route. Parasitemia levels were recorded from thin blood smears at regular intervals of four days throughout the period of experiment. The mean value determined for a group of five mice was used to calculate the percent suppression of parasitemia with respect to the untreated control group. Treatment was considered curative when no parasites were detected till day 28. Mice surviving at day 28 were inoculated with $1x10^6$ *P. yoelii* parasitized RBC to monitor their susceptibility to rechallenge [31]. Mice treated with CQ served as reference controls.

**2.3 Molecular Modeling study:**

**2.3.1 Database Preparation**

Molecular docking study was carried out for in-house CQ analogues by targeting heme. SYBYL-X 1.3 (Tripos Inc, St. Louis, MO, USA) modeling package [32] was used for molecular modeling studies. To execute the docking experiment, in-house database was prepared containing 168 CQ derivatives including recently synthesized molecules which are reported in this paper. All compounds were drawn by using sketch module in sybyl-X 1.3[33]. Structures were minimized further by adding Gasteiger-Huckel charges along with distance-dependent dielectric and the Powell conjugate gradient algorithms with a convergence criterion of 0.001 kcal/mol. All prepared structures were put into a new database and finally aligned with most active molecule (M96) of the present database by 'Fit Atom' method.

**2.3.2 Protomol based docking**

Docking study of synthesized compounds was performed using the Surflex-Dock module with standard protocols in SYBYL-X 1.3 [34]. Since, heme is the primary target of CQ analogues, we have extracted the heme from the protein of *P. falciparum* (PDB ID: 4D6U) to continue the docking experiment [35]. Additionally, CQ was taken as a reference to validate our docking experiment. Extracted heme was further prepared through Surflex-Dock protocol. Hydrogen atoms were added to the heme to define the correct configuration and tautomeric states. Gasteiger-Huckel charges were also added to it followed by energy-minimizations using the Tripos force fields along with distance-dependent dielectric and the Powell conjugate gradient algorithms with a convergence criterion of 0.001 kcal/mol. After the preparation of heme, automated protomol generation process was used to identify the grid for docking. The docking algorithm implemented in SURFLEX uses an idealized active site ligand called a protomol. This protomol is made up of probes representing sites of potential hydrogen bonds and favorable hydrophobic interactions with docking target.

Molecular docking of 168 molecules was performed by placing the molecules including the reference compound CQ into the protomol based grid by an empirical scoring function to score the ligand and protomol guided docking. Finally, the protomol-based method and empirically derived scoring function (e.g. Total score, crash score, polar etc.) were used to calculate the binding affinities. The scoring function comprised hydrophobic, polar, repulsive, entropic, crash and salvation terms. Total score is expressed in -log ($K_d$) units to represent total binding affinities. Higher total score represents good binding affinity. Crash is the degree of inappropriate penetration by the ligand into the protein and of interpenetration (self-clash) between ligand atoms that are separated by rotatable bonds. A smaller crash value (near to zero) indicates a better ability to exclude the false positives screened. Polar represents the

contribution of the polar interactions to the total score. The polar score is useful for excluding docking results that make no hydrogen bonds.

**2.3.3. Data set preparation for 3D-QSAR**

All docked molecules were further used to prepare a 3D-QSAR model to identify important features for antiplasmodial activity. The in-house database of 168 molecules (**Table 1**) along with their *in vitro* antiplasmodial activity (*P. falciparum* 3D7 strain) in the form of logarithm of the inverse of inhibitory concentration (-log$IC_{50}$) were used. For the purpose of CoMFA/CoMSIA analysis dataset has been randomly divided into training set (111 compounds) and test set (57 compounds) (**Table 3**).

**2.3.4. Molecular alignment**

The 3D-structure building and all modelling studies were performed using the SYBYL program package, version 7.3 [36] on a silicon graphics fuel workstation with IRIX 6.5 operating system. In this study conformations of all molecules (168) were taken from previous docking experiment. Out of this, one best conformation (based on Total Score) of compound M96 was identified to execute molecular alignment of all molecules. Before alignment energy minimizations were performed on docked molecules to add charges using the Tripos force field [37] with a distance-dependent dielectric function and the Powell conjugate gradient algorithm with a convergence criterion of 0.05 kcal/mol. Partial atomic charges were calculated using the Gastieger–Huckel method. The most potent compound M96 was chosen as template molecule to fit the remaining training and test compounds by using the ‘‘database align’’ function in SYBYL. The reference atoms in the compound M96 were used for alignment via "fit atom" method which is exposed in **Figure 3**.

**2.3.5. CoMFA and CoMSIA analysis**

In deriving the CoMFA and CoMSIA descriptor fields, a 3D cubic lattice with grid spacing of 1Å and extending to 4Å units beyond the aligned molecules in all directions was created to encompass the aligned molecules. CoMFA descriptors were calculated using an $sp^3$ carbon probe atom with a van der Waals radius of 1.52Å and a charge of +1.0 to generate steric (Lennard–Jones 6–12 potential) field energies and electrostatic (Coulombic potential) fields with a distance-dependent dielectric at each lattice point. Steric and electrostatic fields generated were scaled by the CoMFA-Standard method in SYBYL with default cut-off energy of 30 kcal/mol. The minimum column filtering was set to 2.0 kcal/mol to improve the signal-to-noise ratio by omitting those lattice points whose energy variation was below this threshold. CoMSIA similarity indices were derived according to Klebe *et al.* [38] with the

same lattice box as was used for the CoMFA calculations. CoMSIA similarity indices ($A_F$) for a molecule *j* with atoms *i* at a grid point *q* were calculated using Eq. (1) as follows:

$$A_{F,K}^{q}(j) = -\sum_{i=1}^{n} \omega_{probe,k}\, \omega_{ik} e^{-\alpha r_{iq}^{2}} \qquad (1)$$

The CoMSIA method involves computation of five different physicochemical properties (k) namely steric, electrostatic, hydrophobic, hydrogen bond donor and hydrogen bond acceptor as molecular similarity indices (Eq. 1). The computational use of Gaussian type distance-dependent function was performed between the grid point *q* and each atom *i* in the molecule. A default value of 0.3 was used as the attenuation factor (α). In CoMSIA, the steric indices are related to the third power of the atomic radii; the electrostatic descriptors are derived from partial atomic charges; the hydrophobic fields are derived from atom based parameters [39].

**2.3.6. PLS analysis**

The CoMFA and CoMSIA 3D-QSAR models were derived using the PLS regression procedure of SYBYL [40]. The predictive ability of the model was measured in terms of cross-validated $r^2$ ($r^2_{cv}$ or $Q^2$) as shown in equation 2.

$$r_{cv}^{2} = 1 - \frac{\Sigma (Y_{\text{predicted}} - Y_{\text{observed}})^2}{\Sigma (Y_{\text{observed}} - Y_{\text{mean}})^2} \qquad (2)$$

Where $Y_{\text{predicted}}$, $Y_{\text{observed}}$, and $Y_{\text{mean}}$ are predicted, actual, and mean values of the target property ($pIC_{50}$), respectively. The number of components leading to the lowest standard error of prediction (*SEP*) were used as optimum number of components (ONC) to generate the final PLS regression models. The models were validated through the boot strapping analysis for 100 runs and the cross-validation analysis (leave-half-out and leave 20% out; each 50 runs) [40]. The CoMFA and CoMSIA equations were plotted as contour maps to express the percentage contribution of respective fields to the activity. This was done by considering the field energies at each lattice point as a multiple of the regression coefficient and corresponding standard deviation. Here, the contour maps help in identifying the important regions where changes may affect the binding preference and thereby facilitate the recognition of key features contributing to the interactions between the ligand and the active site of a receptor. Furthermore, the developed CoMFA and CoMSIA models were validated by predicting the activity of the external test set compounds. A model with predictive $r^2$ value ($r^2_{pred}$) more than 0.5 may be considered as statistically significant.

## 3. Results and Discussion

### 3.1. *In vitro* antiplasmodial activity

All compounds synthesized in the present study **6a-6d**, **7a-7h**, **8a-8d**, **9a-9d**, **10a-10b**, **11a-11c** and **12a** were evaluated for antiplasmodial activity against the 3D7-chloroquine sensitive (CQ-S) and K1-chloroquine resistant (CQ-R) strains of *P. falciparum* according to the procedure reported by Kondaparla *et al*. [26]. Selected compounds (**6b**, **6d**, **7c**, **7h**, **8c**, **8d**, **9a** and **9c**), showing superior activity than CQ against the K1 strain, were evaluated for *in vivo* activity against the innately chloroquine resistant *P. yoelii* (N-67 strain) in Albino mice of Swiss strain. All tested compounds displayed moderate activity with $IC_{50}$ value ranging from 22.61 to >5000 nM against 3D7 strain. In all tested compounds, two compounds (**7d** &**7h**) showed promising activity with an $IC_{50}$ of 24.55 and 22.61nM, and three compounds (**6a**, **7c** & **9a**) with $IC_{50}$ values ranging from 56.98 nM to 108.39 nM showed moderate activity. Moreover, eight compounds of the series were discerned to be more active ($IC_{50}$ 46.50 to 161.80 nM) than CQ ($IC_{50}$ = 255 nM) against the CQ resistant strain of *P. falciparum*. Three compounds **6a**, **7e** and **9b** exhibited $IC_{50}$ values 276.90, 352.30 and 362.28 nM than the CQ, respectively. Moreover, low resistance index was exhibited by majority of the synthesized compounds (**Table 1**). *In vitro* biological activity data of the synthesized compounds are summarized as shown in **Figure 2.**

The structure activity relationship studies on these compounds suggested that the activities were greatly influenced by the type of substitutions at $4^{th}$ position of piperazine moiety, structural diversity in the amino acid side chain and trifluoromethyl substitution at C-7 position of the quinoline ring. More importantly, substitution at the piperazine moiety showed remarkable influence on the antiplasmodial activity.

The results presented in **Table1** indicate that the compounds having ethyl, benzyl and piperonyl group at the $4^{th}$ position of piperazine (irrespective of amino acid side chain) exhibited mild inhibition against the 3D7 strain and superior activity against the K1 strain of *P. falciparum* as compared to CQ. However, compound **7c** showed 2.6 fold more activity than CQ against the K1 strain with $IC_{50}$ value 97.76 nM . Further, replacement of chlorine in **7c** with trifluoromethyl gave the compound **7d** ($IC_{50}$ = 797.67 nM) with many fold decrease in the activity against the K1 strain. This decrease in the activity may be due to increase in the hydropobicity. Again, the activity was increased substantially against the K1 strain in the case of compound **7h (**$IC_{50}$ = 46.52 nM (K1)) which is having piperonyl methyl substitution in the side chain. It is important to note that this compound was found 5.5 fold more active than CQ against the K1 strain. When the amino acid side chain was changed to the hydrophobic benzyl group it furnished the compounds with considerable decrease in the

activity against the K1 strain of *P. falciparum*. However, compound **8c** ($IC_{50}$ = 70.82 nM) with similar substitution as in the case of compound **7c** ($IC_{50}$ = 97.76 nM) exhibited slight increase in the activity against the K1 strain. Similar activity profile was observed with piperonyl methyl substitution in the case of compound **8d** ($IC_{50}$ = 89.0 nM). Moreover, compound **6d** ($IC_{50}$ = 46.50 nM) having glycine at $4^{th}$ position of quinoline ring showed better activity than the compound **9a** ($IC_{50}$ = 71.39 nM) having alanine at the same position. More importantly, these two compounds exhibited 5.5 fold and 3.6 fold superior activities respectively, than CQ against the K1 strain of *P. falciparum*. The chance of parasite to develop resistance to a particular class of compounds has been calculated as a ratio of $IC_{50}$ in CQ-Resistance *vs* CQ-Sensitive strains called resistance factor (RI). Therefore, smaller resistance factor of the given compound corresponds to less chance of developing resistance. Interestingly, the majority of tested compound in this series exhibited low resistance factor between 0.08 and 32.49 as compared to 51 for CQ. Furthermore, the better antiplasmodial activity has been accounted in compounds of present study against both CQ-S and CQ-R strains in comparison to the earlier reported antimalarial activity from our laboratory. In the light of current study, tested compounds seem to suggest further lead optimization to obtain active molecule against drug resistant parasites.

### 3.2. *In vitro* inhibition of *β*-hematin formation

Newly synthesised 4-aminoquinolines (**6a-6d**, **7a-7h**, **8a-8d**, **9a-9d**, **10a-10b**, **11a-11c** and **12a**) were evaluated for their mode of action using the reported method [19] and the results are given in **Table 1**. The heme binding assay results revealed that all synthesised 4-AQ's derivatives interact with the heme. Further, association constant was observed in the range of 4.23-7.81. These results indicate that interaction between quinoline ring and the porphyrin ring system might be π–π stacking interaction. These results are complemented by the inhibition of *β*-hematin formation which also showed good $IC_{50}$ values found in the range of 0.21–0.83 µM. In the present series the most active compound **7h** exhibited $IC_{50}$ 0.21 µM against the CQ-R strain.

### 3.3. *In vitro* Cytotoxicity

MTT assay in VERO cell line was used to determine the cytotoxicity of all synthesized compounds (**6a-6d, 7a-7h, 8a-8d, 9a-9d, 10a-10b, 11a-11c** and **12a**) (**Table 1**). The selectivity index (SI) of nearly all compounds in series is good and ranging between 32.77 and 3671.69. Compounds **7c, 7h** and **9a** of the series showed enhanced antiplasmodial activities against K1 strain and also exhibit good selectivity SI values 3510, 582.04 and 117.94, respectively. However, compounds **6a, 9b** and **12a** displaying promising activities

against the K1 strain also showed considerable SI values 979.10, >1580.52 and 1093.10 respectively. Moreover within series of compounds, compounds **7d** and **7h** showed significant activity against the 3D7 strain with good SI value 3671.69 and 582.04, respectively. In general, with promising activity against the K1 strain, less cytotoxic effect and fairly high selectivity index, most of the 4-aminoquinoline derivatives of this series are very healthy candidate for further lead optimization.

### 3.4. *In vivo* antimalarial activity

The *in vivo* antimalarial activity was assessed against inherently chloroquine resistant *P. yoelii* (N-67 strain) in Albino mice of Swiss strain. Compounds (**6b**, **6d**, **7c**, **7h**, **8c**, **8d**, **9a**, **9c**) with $IC_{50}$ ranging between 31.19 nM and 252.28 nM were selected based on *in vitro* antiplasmodial activity. In the beginning, the *in vivo* activities of selected compounds were examined at the dose of 100mg/kg for four consecutive days, once daily via oral route. Parasitaemia reduction and survival of animals were recorded until day 28 post-infection (**Table 2**).

A dose of 100 mg/kg compounds 6b, 6d, 8d, 9a and 9c showed 100% parasitaemia suppression on day 4 but no mice of the group was cured up to day 28 of treatment. Further, compound **8c** was administered at two different doses such as 100 and 50 mg/kg, respectively. At a dose of 100 mg/kg it displayed 100% parasitaemia suppression on day 4 with 100% survival and curative rates up to day 28. Whereas, at a dose of 50 mg/kg exhibited 50% parasitaemia suppression on day 4 with 40% survival rate up to day 28 of treatment. Moreover, compound **7c** one of the potent compounds in the series tested initially at a dose of 100 mg/kg, showed 100% survival as well as curative rates up to day 28. When it was administered at lower doses, 50, 25, 12.5 and 6.25 mg/kg, respectively, it displayed 100% parasitaemia suppression on day 4 with 100% curative rate up to day 28 at doses of 50, 25 and 12.5 mg/kg, respectively. While, at a dose of 6.25 mg/kg showed 100% parasitaemia suppression on day 4 but none of the mice survived. Re-inoculation with infective inoculum post day 28 showed that all the cured group mice developed fulminating parasitemia and succumbed to infection thus validating absence of any latent parasites in these animals. In contrast surviving animals which were not designated as cured survived the re-challenge (Table 2).

### 3.5. Molecular docking studies

Recent evidence strongly leans towards interaction of CQ analogues with the surface of the hemozoin crystal, rather than free heme [41-42]. Understandably, this is difficult to make a model of hemozoin structure for docking. Therefore, the in-house database created in the present study (168 molecules) was used to dock against the heme instead of hemozoin, (extracted from PDB ID: 4D6U) to investigate the probable interactions between CQ analogues and the heme. Docking analysis of these molecules clearly showed the importance of total score, crash score and polar scores (**Table 4**).

Most of the compounds showed moderate to good binding scores with the heme. Compounds M64, M96, M97 and M100 confirmed good binding affinity with the heme due to strong H-bond interactions with free carboxylic group of the heme moiety (**Figure 4**) whereas compounds M32, M158, M165 showed poor binding affinity towards the heme due to improper binding conformations. This is in agreement with the observed biological activity.

Additionally, excellent electrostatic and hydrophobic (π-π stacking) interactions between quinoline ring and the porphyrin ring of the heme moiety contribute significantly to improve the binding affinities (**Figure 5, Table 5**) which are directly linear to their biological activity against the 3D7 strain (**Table 1** & **4**). Furthermore from the above observation, it is concluded that compounds with more bulky groups in side chains (compound M153, M161 and M165) poorly bind with the heme which is reflected through their maximum crash score value and unfavourable docked conformations due to the lack of π-π stacking interactions. In addition, docking analysis further revealed that low polar score may reduce the formation of good heme-ligand complex (compound M37, M153 and M157) leading to reduced activity (**Figure 4**). These results revealed the importance of the side chain modifications to improve the binding affinity of CQ analogues towards heme.

**3.6. CoMFA and CoMSIA Statistical analysis**:

The best possible 3D-QSAR model is derived from the PLS statistical data of CoMFA and CoMSIA for CQ analogues which is shown in **Table 6**. The optimal value of $Q^2$ (> 0.5) was used as criteria to find out new significant model. The ideal CoMFA model has been recognized with five PLS components along with cross-validated $Q^2$ value of 0.641, non-cross validated $r^2$ value of 0.924 and $r^2_{pred}$ = 0.656 (**Table 6**). In the case of CoMSIA study, five components were established to ideally express the anti-malarial activity of the compounds. It has revealed a cross-validated $Q^2$ of 0.680 and a non-cross validated $r^2$ of 0.885. In CoMSIA also good predictive value is identified ($r^2_{pred}$ = 0.608) with test sets.

The 3D-QSAR model derived from this experiment has shown that all five fields of CoMSIA do not equally play a vital role to explain the activity. Therefore, single as well as multiple groupings of CoMSIA fields have been measured to choose the important fields with best cross-validated $Q^2$ value. Finally, from this experiment most important fields responsible for activity are recognized, namely steric, electrostatic and hydrophobic fields (**Figure 6**).

3D models of CoMFA and CoMSIA are found to be effective in bootstrapping and other cross-validation experiments (**Table 6**). Moreover, derived model predicted the test set of compounds satisfactorily. The scattered graphical plots of observed *vs* predicted values of biological activities of training and test groups resulting from the CoMFA and CoMSIA study are revealed in **Figure 7**.

### 3.7. Contour map analysis

#### 3.7.1. CoMFA Steric

The CoMFA steric contour maps of CQ derivatives against 3D7 strain are exposed in **Figure 7**. Here, green and yellow colour contours correspondingly specified the steric favoured as well as unfavoured regions for the activity. Green contour present at linker region (**Figure 8**) identify the sterically preferred groups in this area to get improved anti-malarial activity as observed in the compound M96. In addition, green contour close to the end of linker site (**Figure 8**) indicates the positivity of this location for steric groups. All active analogues (Compounds M64, M96, M98 and M126) satisfy this criteria with different steric groups such as *tert*-butyl, methyl piperazine and methyl piperidine moieties. Similarly, yellow contours are situated at C-7 position of the quinoline ring (**Figure 8**). Another yellow contour has enclosed more bulky groups at linker region (Compounds M32, M34 and M68 **Figure 8**). This speaks in favour of least steric groups at C-7 position.

#### 3.7.2. CoMFA Electrostatic

The electrostatic contour map build up for CQ derivatives from CoMFA model is shown in **Figure 8**. In this, a large blue colour contour adjacent to the electropositive 4-amino of quinoline group indicate the presence of electron rich nitrogen which may increase the activity (Compounds M60, M62, M96 and M97). Additionally another small blue contour near to the linker site specifies its requirement for electropositive groups. Apart from that, a red colour contours are observed near to linker site in the case of less active compounds (**Figure 8**, Compound M146, M149 and M161). Therefore, electronegative groups can be replaced at linker region with electropositive moieties to improve their activity. Moreover, a blue contour is positioned in front of quinoline moiety representing the prominence of electropositive groups for the biological activity.

**3.7.3. CoMSIA Steric**:

In CoMSIA, the favourable areas for steric groups are indicated in green contour and the disfavoured regions are represented in yellow colour contour. At this point, two large green contours occurred in proximity to linker (chain) sides indicating the fitness for large groups in these positions. The presence of *tert*-butyl, methyl piperazine and like moieties appears to be favourable for good activity (e.g. compounds M64, M96 and M97). The substituted piperazine moiety has fulfilled the steric requirements of the green contour parallel to linker region (**Figure 9**, compound M96). Most of the active compounds in the dataset contribute to this feature (e.g. compounds M96, M100 and M109). Besides this, two yellow big contours were found over the green contour suggesting the presence of large groups in this area which can diminish the activity (compounds M32, M158 and M165).

**3.7.4. CoMSIA Electostatic**

In this electrostatic map blue colour contours specified the electropositive favourable area and red colour contours pointed out electronegative favourable sites. The blue contour existed close to the linker region (**Figure 9**) which suggested that electropositive groups are suitable for the activity (compounds M60, M62, M96 and M97). In case of active compounds, this position is fulfilled by methyl ethyl amine and methyl piperazine groups. Incorporation of alkyl chains in this electropositive region improves the activity but red contour map near to this region drastically reduces the biological activity (compounds M146, M149 and M161).

**3.7.5. CoMSIA Hydrophobic**

The CoMSIA hydrophobic contour maps are shown in **Figure 9**. In these contours, yellow colour specified hydrophobic favourable regions whereas gray colour specified for hydrophobic unfavourable sites. The yellow contour near to the linker position showed the positive site for hydrophobic groups (compounds M63, M64, M96 and M100). In highly active compounds dimethyl amine, *tert*-butyl, methyl piperazine and other related groups were incorporated in this region. Perhaps, the hydrophobic part of these groups along with other characteristics may be appropriate for this position. Apart from this, a large gray contour and a small gray contour occupied the central area of linker region and C-7 position of the quinoline ring, respectively. This denoted an adverse environment for hydrophobic moieties in the surrounding area of mid part of the linker position as well as C-7 position of the quinoline ring system (compounds M32, M108 and M167).

**4. Conclusion**

In summary, we have synthesised a new series of chiral 4-aminoquinoline derivatives in order to search for more potent molecules active against both *in vitro* and *in vivo* strains of *P. falciparum*. Among all synthesised compounds, eight compounds (**6b**, **6d**, **7c**, **7h**, **8c**, **8d**, **9a** and **9c**) exhibited excellent antimalarial activity against the K1 strain as compared to the CQ and these compounds were also found to be active against *P. yoelii* mouse model *in vivo*. It may be inferred from the above mentioned results that the less hindered amino acids (namely Gly, Ala and Leu) at $4^{th}$ position of the quinoline ring and ethyl substituted piperazine in the side chain exhibited potent activity as a new lead and requires further optimization for drug development. The docking as well as 3D-QSAR studies were performed to make SAR on our in-house 4-aminoquinoline derivatives data set. After exploration, it is clear that *H*-bond as well as hydrophobic π-π stacking interactions between quinoline ring and porphyrin moiety of the heme is crucial for antimalarial activity. Also, the CoMFA/CoMSIA outcomes mostly pointed out the influence of steric, hydrophobic and electropositive environment creating groups adjacent to the linker attached to the quinoline moiety for their potential activity against *P. falciparum*. The steric field around the linker site is most crucial to enhance the biological activity. The end part of the linker region is suitable for steric, hydrophobic and electropositive groups as well. Apart from that, C-7 position of quinoline ring specified the significance of minimum hydrophobicity and least steric influence for the activity. The present *in silico* experiments with the newly synthesized compounds offered support to the biological activities. Therefore, it is expected that the present study will provide a new way to design and synthesize novel CQ analogues having antimalarial activity against drug resistant malaria paasite.

**Acknowledgements**

S. Kondaparla and U. Debnath are thankful to the CSIR, New Delhi, for a Senior Research Fellowship. We thank the director of CSIR-CDRI for support and the SAIF division for the spectral data. Authors are also thankful to Dr. R K Rawal for his advice. CSIR-CDRI Communication no. is 9731.

**Conflict of interest**

The authors declare that no competing interests exist.

**References:**


1. Schlitzer, M. Malaria chemotherapeutics part I: History of antimalarial drug development, currently used therapeutics, and drugs in clinical development. *Chem. Med. Chem.* **2007,** 2, 944-86.

2. World Health Organization's World Malaria Report **2016**; www.who.int

3. Dola, V. R.; Kondaparla, S.; Katti, S. B. Recent developments in the side chain modified 4-aminoquinolines as antimalarial agents. *Chem. Biolo. Interface*. **2014**, 4, 206-22.

4. O'Neill, P. M.; Bray, P. G.; Hawley, S. R.; Ward, S. A.; Park, B. K. 4-Aminoquinolines--past, present, and future: a chemical perspective. *Pharmacol Ther* **1998,** 77, 29-58.

5. Rodrigues, T.; Moreira, R.; Lopes, F. New hope in the fight against malaria? *Future Med Chem* **2011,** 3, 1-3.

6. Read, J. A.; Wilkinson, K. W.; Tranter, R.; Sessions, R. B.; Brady, R. L., Chloroquine binds in the cofactor binding site of Plasmodium falciparum lactate dehydrogenase. *The J. Biol. Chem* **1999,** 274 (15), 10213-8.

7. Hawley, S. R.; Bray, P. G.; Mungthin, M.; Atkinson, J. D.; O'Neill, P. M.; Ward, S. A. Relationship between antimalarial drug activity, accumulation, and inhibition of heme polymerization in Plasmodium falciparum in vitro. *Antimicrob Agents Chemother* **1998,** 42, 682-6.

8. Bray, P. G.; Howells, R. E.; Ritchie, G. Y.; Ward, S. A. Rapid chloroquine efflux phenotype in both chloroquine-sensitive and chloroquine-resistant Plasmodium falciparum. A correlation of chloroquine sensitivity with energy-dependent drug accumulation. *Biochem Pharmacol* **1992,** 44, 1317-24.

9. De, D.; Krogstad, F. M.; Byers, L. D.; Krogstad, D. J. Structure-activity relationships for antiplasmodial activity among 7-substituted 4-aminoquinolines. *J Med Chem* **1998,** 41, 4918-26.

10. Burgess, S. J.; Kelly, J. X.; Shomloo, S.; Wittlin, S.; Brun, R.; Liebmann, K.; Peyton, D. H. Synthesis, structure-activity relationship, and mode-of-action studies of antimalarial reversed chloroquine compounds. *J Med Chem* **2010,** 53, 6477-89.

11. Ridley, R. G.; Hofheinz, W.; Matile, H.; Jaquet, C.; Dorn, A.; Masciadri, R.; Jolidon, S.; Richter, W. F.; Guenzi, A.; Girometta, M. A.; Urwyler, H.; Huber, W.; Thaithong, S.; Peters, W. 4-aminoquinoline analogs of chloroquine with shortened side chains retain activity against chloroquine-resistant Plasmodium falciparum. *Antimicrob Agents Chemother* **1996,** 40, 1846-54.

12. O'Neill, P. M.; Ward, S. A.; Berry, N. G.; Jeyadevan, J. P.; Biagini, G. A.; Asadollaly, E.; Park, B. K.; Bray, P. G. A medicinal chemistry perspective on 4-aminoquinoline antimalarial drugs. *Curr Top Med Chem* **2006,** 6, 479-507.

13. Natarajan, J. K.; Alumasa, J. N.; Yearick, K.; Ekoue-Kovi, K. A.; Casabianca, L. B.; de Dios, A. C.; Wolf, C.; Roepe, P. D. 4-N-, 4-S-, and 4-O-chloroquine analogues: influence of side chain length and quinolyl nitrogen pKa on activity vs chloroquine resistant malaria. *J Med Chem* **2008,** 51, 3466-79.

14. Kaur, K.; Jain, M.; Reddy, R. P.; Jain, R. Quinolines and structurally related heterocycles as antimalarials. *Eur J Med Chem* **2010,** 45, 3245-64.

15. Solomon, V. R.; Haq, W.; Srivastava, K.; Puri, S. K.; Katti, S. B. Synthesis and antimalarial activity of side chain modified 4-aminoquinoline derivatives. *J Med Chem* **2007,** 50, 394-8.

16. Solomon, V. R.; Puri, S. K.; Srivastava, K.; Katti, S. B. Design and synthesis of new antimalarial agents from 4-aminoquinoline. *Bioorg Med Chem* **2005,** 13, 2157-65.

17. Solomon, V. R.; Haq, W.; Smilkstein, M.; Srivastava, K.; Puri, S. K.; Katti, S. B. 4-Aminoquinoline derived antimalarials: synthesis, antiplasmodial activity and heme polymerization inhibition studies. *Eur J Med Chem* **2010,** 45, 4990-6.

18. Dola, V. R.; Soni, A.; Agarwal, P.; Ahmad, H.; Raju, K. S.; Rashid, M.; Wahajuddin, M.; Srivastava, K.; Haq, W.; Dwivedi, A. K.; Puri, S. K.; Katti, S. B. Synthesis and Evaluation of Chirally Defined Side Chain Variants of 7-Chloro-4-Aminoquinoline To Overcome Drug Resistance in Malaria Chemotherapy. *Antimicrob Agents Chemother* **2017,** 61.

19. Kondaparla, S.; Soni, A.; Manhas, A.; Srivastava, K.; Puri, S. K.; Katti, S. B. Synthesis and antimalarial activity of new 4-aminoquinolines active against drug resistant strains. *RSC Adv* **2016**, 6, 105676-89.

20. Sinha, M.; Dola, V. R.; Agarwal, P.; Srivastava, K.; Haq, W.; Puri, S. K.; Katti, S. B. Antiplasmodial activity of new 4-aminoquinoline derivatives against chloroquine resistant strain. *Bioorg Med Chem* **2014,** 22, 3573-86.

21. Kondaparla, S.; Agarwal, P.; Srivastava, K.; Haq, W.; Puri, S. K.; Katti, S. B. Design, synthesis and in vitro antiplasmodial activity of 4-aminoquinolines containing modified amino acid conjugates. *Med Chem Res* **2016**, 25, 1148-62.

22. Ryckebusch, A.; Deprez-Poulain, R.; Maes, L.; Debreu-Fontaine, M. A.; Mouray, E.; Grellier, P.; Sergheraert, C. Synthesis and in vitro and in vivo antimalarial activity of N1-(7-chloro-4-quinolyl)-1,4-bis(3-aminopropyl)piperazine derivatives. *J Med Chem* **2003,** 46, 542-57.

23. Sinha, M.; Dola, V. R.; Soni, A.; Agarwal, P.; Srivastava, K.; Haq, W.; Puri, S. K.; Katti, S. B. Synthesis of chiral chloroquine and its analogues as antimalarial agents. *Bioorg Med Chem* **2014,** 22, 5950-60.

24. Soal, A.; Oyamada, H.; Takase, M. The preparation of N-protected amino alcohols and N-protected peptide alcohol by reduction of the corresponding esters with sodium borohydride. An improved procedure involving a slow addition of a small amount of methanol. *Bull Chem Soc Jpn,* **1984,** 57, 2327-28.

25. Kenyon, RL.; Wiesner, JA.; Kwartler, CE. Chloroquine manufacture. *Ind Eng Chem* **1949**, *41*, 654-62.

26. Kondaparla, S.; Soni, A.; Manhas, A.; Srivastava, K.; Puri, S. K.; Katti, S. B. Antimalarial activity of novel 4-aminoquinolines active against drug resistant strains. *Bioorg Chem* **2017,** 70, 74-85.

27. Pagola, S.; Stephens, W. P.; Bohle, D. S.; Kosar, A. D.; Madsen, S. K. The structure of malaria pigment β-haematin. *Nature* **2000**, 404, 307-10.

28. Tripathi, A. K.; Khan, S. I.; Walker, L. A.; Tekwani, B. L. Spectrophotometric determination of de novo hemozoin/beta-hematin formation in an in vitro assay. *Anal Biochem* **2004,** 325, 85-91.

29. GraphPad Prism, version 3.0, GraphPad Software, 10855 Sorrento Valley Rd.

#203, San Diego, CA 92121, **1999.**

30. Cheng, J.; Zeidan, R.; Mishra, S.; Liu, A.; Pun, S. H.; Kulkarni, R. P.; Jensen, G. S.; Bellocq, N. C.; Davis, M. E. Structure-function correlation of chloroquine and analogues as transgene expression enhancers in nonviral gene delivery. *J Med Chem* **2006,** 49, 6522-31.

31. Gumila, C1.; Ancelin, ML.; Delort, AM.; Jeminet, G.; Vial, HJ.; Characterization of the potent in vitro and *in vivo* antimalarial activities of ionophore compounds. *Antimicrob Agents Chemother*. **1997,** 41, 523-29.

32. Tripos Associates: SYBYL Molecular Modelling Software, version X. St. Louis, MO: Tripos Associates; 2009. Technical tips online. Available at http://www.tripos.com.

33. Verma, S; Debnath, U.; Agarwal, P.; Srivastava, K.; Prabhakar, Y.S. In Silico exploration for new antimalarials: Arylsulfonyloxy acetimidamides as Prospective Agents. *J Chem Inf Model.* **2015,** 55*,* 1708-19.

34. SYBYL, version 7.3, **2006**, Tripos Associates, St. Louis, MO, USA.

35. Capper, M. J.; O'Neill, P.M.; Fisher, N.; Strange, R.W.; Moss, D.; Ward, S.A.; Berry, N.G.; Lawrenson, A. S.; Hasnain, S. S.; Biagini, G. A.; Antonyuk, S. V. Antimalarial 4(1H)-Pyridones Bind to the Qi Site of Cytochrome Bc1. *Proc.Natl.Acad.Sci.USA*, **2015**,112,755-60.

36. Clark, M.; Cramer, R. D.; Opdenbosch, N.V. Validation of the general-purpose tripos 5.2 force field. *J Comput Chem* **1989**, 10, 982-12.

37. Klebe, G.; Abraham, U.; Mietzner, T. Molecular similarity indices in a comparative analysis (CoMSIA) of drug molecules to correlate and predict their biological activity. *J Med Chem* **1994,** 37, 4130-46.

38. Klebe, G. The use of composite crystal-field environments in molecular recognition and the de novo design of protein ligands. *J Mol Biol* **1994,** 237, 212-35.

39. Stahle, L.; Wold, S. Multivariate data analysis and experimental design in biomedical research. *Prog Med Chem* **1988,** 25, 291-338.

614 40. Debnath, U.; Verma, S.; Jain, S.; Katti, S. B.; Prabhakar, Y. S. Pyridones as NNRTIs
615 against HIV-1 mutants: 3D-QSAR and protein informatics. *J Comput Aided Mol Des*
616 **2013,** 27, 637-54.

617 41. Schwedhelm, K.; Horstmann, M.; Faber, J.; Reichert, Y.; Buchner, M.; Bringmann,
618 G.; Faber, C. Spin State of Chloroquine-Heme Complexes: Formation of a Hemin
619 Tetramer Adduct. *The Open Spectroscopy Journal*, **200**8, 2, 10-18.

620 42. Solomonov, I.; Osipova, M.; Feldman, Y.; Baehtz, C.; Kjaer, K.; Robinson, I. K.;
621 Webster, G. T.; McNaughton, D.; Wood, B. R.; Weissbuch, I.; Leiserowitz, L. Crystal
622 Nucleation, Growth, and Morphology of the Synthetic Malaria Pigment β-Hematin
623 and the Effect Thereon by Quinoline Additives: The Malaria Pigment as a Target of
624 Various Antimalarial Drugs. *J. Am. Chem. Soc.*, **2007**, 129, 2615–2627

625

626 **Captions**

627 **Table 1**

628 Biological and biophysical data of the synthesized compounds.

629 **Table-2**

630 *In vivo* antiplasmodial activity of selected compounds against CQ resistant *P. yoelii* (N-67)
631 in Albino mice of Swiss strain.

632 **Table-3**

633 Distribution pattern of 4-aminoquinoline derivatives in training and test sets

634 **Table 4**

635 Binding scores (Total Score, Crash Score & Polar Score) of selected molecules from the in
636 house database.

637 **Table 5**

638 Different types of non h-bond interactions between heme and CQ analogue (M96).

639 **Table 6**

640 Goodness of fit of CoMFA and CoMSIA model for the antiplasmodial activities of
641 chloroquine (CQ) analogues against 3D7 strain.

642 **Figure 1**

643 Synthesis of compounds **(6a-6d**, **7a-7h**, **8a-8d**, **9a-9d**, **10a**, **11a-11c**, and **12a)**

644

**Figure 2**

Histogram showing the number of compounds evaluated against *P. falciparum* in the present study.

**Figure 3**

General structures of the all synthesized compounds. The asterisk marked the atoms which are common to all structures and used for the CoMFA/CoMSIA alignment.

**Figure 4**

Molecular docking of most active ('A': M96, 'B': M64 and 'C': M62) and less active ('D': M32, 'E': M158 and 'F': M165) compounds with heme. Red colour (---) indicate h-bond interaction.

**Figure 5**

Non h-bond interactions between heme and M96. Yellow colour (---) indicate electrostatic interactions whereas pink colours (---) indicate hydrophobic interactions.

**Figure 6**

A graphical Plots of $Q^2$ values of CoMSIA models which indicated single as well as multiple field combinations for CQ analogues as antiplasmodial inhibitors against the 3D7 strain. In this plot, x-axis indicate the fields of CoMSIA with single letters i.e. A (HB-Acceptor), D (HB-donor), E (electrostatic), H (hydrophobic) and S (steric). The field combinations which led to the model with ideal $Q^2$ (y-axis) is marked with circle.

**Figure 7**

The scatter plots of experimental $pIC_{50}$ values versus predicted $pIC_{50}$ values derived from CoMFA/CoMSIA training (filled box) and the test set (triangle) of CQ derivatives for Plasmodium falciparum 3D7 strain.

**Figure 8**

Two different contour maps including Steric field contour maps (**A&B**), & electrostatic field contour maps(**C&D**) of CoMFA 3D-QSAR are appeared for CQ analogues as antiplasmodial inhibitors against 3D7 strain. In this figure, the poses of compounds **M96 (active)** & **M32 (inactive)** are used to demonstrate the contour maps. Colour code specified favourable & unfavourable regions. Here, green contours indicate sterically favourable regions and yellow contours shows sterically unfavourable regions for the biological activity (A&**B**). Again, blue contours indicate electropositive regions & red contours pointed out the electronegative regions (**C&D**).

**Figure 9**

Three different contour maps including Steric field contour maps (**A&B**), electrostatic field contour maps(**C&D**) and hydrophobic contour maps (**E&F**) of CoMSIA 3D-QSAR are appeared for CQ analogues as antiplasmodial inhibitors against 3D7 strain. In this figure, the poses of compounds **M96 (active)** & **M32 (inactive)** are used to demonstrate the contour maps. Colour code specified favourable & unfavourable regions. Here, green contours indicate sterically favourable regions and yellow contours shows sterically unfavourable regions for the biological activity (A&**B**). Similarly, blue contours indicate electropositive regions & red contours pointed out the electronegative regions (**C&D**). Again, yellow contours designate hydrophobic favourable regions whereas white contours indicate hydrophobic unfavourable regions for the activity (**E&F**).

***Table 1 Biological and biophysical data of the synthesized compounds.***

| Cmpd.No | $IC_{50}$(nM)[a] | | Resistance factor[b] | SI[c] | LogK[d] | $IC_{50}$(µM)[e] |
|---|---|---|---|---|---|---|
| | 3D7 | K1 | | | | |
| **6a (M144)** | 108.39 | 276.90 | 2.54 | 979.10 | 5.85±0.03 | 0.38±0.02 |
| **6b(M146)** | 899.23 | 161.80 | 0.17 | 69.6 | 4.72±0.02 | 0.41±0.01 |
| **6c(M149)** | 993.50 | 4231 | 4.26 | 61.5 | 6.33±0.03 | 0.69±0.03 |
| **6d(M161)** | 521.20 | 46.50 | 0.08 | 43.28 | 4.23±0.03 | 0.23±0.01 |
| **7a** | 123.53 | >1000 | >8.09 | 174.70 | 6.63±0.02 | 0.73±0.01 |
| **7b** | 153.90 | >1000 | >6.49 | 292.90 | 6.43±0.01 | 0.69±0.02 |

| | | | | | | |
|---|---|---|---|---|---|---|
| **7c(M140)** | 56.98 | 97.76 | 1.73 | 3510.0 | 4.41±0.02 | 0.27±0.01 |
| **7d(M164)** | 24.55 | 797.67 | 32.49 | 3671.69 | 5.52±0.03 | 0.79±0.03 |
| **7e(M141)** | 460.05 | 352.30 | 0.76 | 90.90 | 6.71±0.02 | 0.44±0.02 |
| **7f(M142)** | 857.68 | 412.40 | 0.48 | 76.60 | 6.31±0.01 | 0.45±0.02 |
| **7g(M143)** | 211.10 | 452.80 | 2.14 | 153.50 | 6.53±0.02 | 0.48±0.03 |
| **7h(M165)** | 22.61 | 46.52 | 2.05 | 582.04 | 4.32±0.02 | 0.21±0.02 |
| **8a(M150)** | >1000 | 1100 | 1.10 | 724.03 | 6.82±0.01 | 0.51±0.01 |
| **8b(M151)** | >5000 | >5000 | 1.00 | ND | 7.81±0.02 | 0.73±0.03 |
| **8c(M152)** | 427.89 | 70.82 | 0.16 | 66.81 | 4.51±0.01 | 0.23±0.01 |
| **8d(M153)** | 757.38 | 89.0 | 0.11 | 61.47 | 4.48±0.02 | 0.29±0.02 |
| **9a(M154)** | 108.10 | 71.39 | 0.65 | 117.94 | 4.53±0.03 | 0.26±0.01 |
| **9b(M155)** | 126.54 | 362.28 | 2.87 | >1580.52 | 5.98±0.03 | 0.42±0.03 |
| **9c(M156)** | 404.80 | 84.01 | 0.20 | 112.69 | 4.42±0.02 | 0.27±0.01 |

| | | | | | | |
|---|---|---|---|---|---|---|
| **9d(M157)** | 538.59 | 783.73 | 1.45 | 40.34 | 5.12±0.03 | 0.48±0.02 |
| **10a(M158)** | 4150.08 | >5000 | 1.20 | ND | 6.97±0.03 | 0.81±0.03 |
| **10b(M160)** | 596.52 | 528.72 | 0.88 | 32.77 | 6.23±0.02 | 0.49±0.01 |
| **11a(M159)** | >5000 | >5000 | 1.00 | ND | 7.13±0.02 | 0.83±0.02 |
| **11b(M162)** | 3099.19 | >5000 | 1.61 | ND | 6.92±0.03 | 0.79±0.03 |
| **11c(M163)** | 2659 | >5000 | 1.88 | ND | 6.96±0.03 | 0.75±0.02 |
| **12a(M145)** | 113.76 | 502.10 | 4.44 | 1093.10 | 5.84±0.02 | 0.49±0.03 |
| **CQ** | 5 | 255 | 51 | 8983 | 5.52±0.02 | 0.17±0.02 |

*[a] $IC_{50}$ (nM): Concentration corresponding to 50% growth inhibition of the parasite; [b]Resistance factor (RI) = $IC_{50}$ (K1)/$IC_{50}$ (3D7); [c]Selectivity index (SI): ($CC_{50}$ for cytotoxicity to vero cells/$IC_{50}$(3D7) for antiplasmodial activity);[d] 1:1 (compound: Hematin) complex formation in 40% aqueous DMSO, 20 mM HEPES buffer, pH 7.5 at 25 ˚C (data are expressed as mean ± SD from at least three different experiments in triplicate); [e]The $IC_{50}$ represents the millimolar equivalents of test compounds, relative to hemin, required to inhibit β-hematin formation by 50% (data are expressed as mean ± SD from at least three different experiments in triplicate).ND: Not done.*

709 ***Table 2: In vivo antiplasmodial activity of selected compounds against CQ resistant* P.**
710 **yoelii *(N-67) in Albino mice of Swiss strain.***

| Compound | Dose (mg/kg [x indicated time]) (p.o)[c] | % suppression on day 4 | Survival[a] | Cure[b] | Survival after rechallenge[d] |
|---|---|---|---|---|---|
| **6b(M146)** | 100 x 4 days | 100 | 0/5 | 0/5 | - |
| **6d(M161)** | 100 x 4 days | 100 | 2/5 | 0/5 | 2/5 |
| **7c(M140)** | 100 x 4 days | 100 | 5/5 | 5/5 | 0/5 |
| | 50 x 4 days | 100 | 5/5 | 5/5 | 0/5 |
| | 25 x 4 days | 100 | 5/5 | 5/5 | 0/5 |
| | 12.5 x 4 days | 100 | 5/5 | 5/5 | 0/5 |
| | 6.25 x 4 days | 100 | 2/5 | 0/5 | 2/5 |
| **7h(M165)** | 100 x 4 days | 100 | 5/5 | 5/5 | 0/5 |
| | 50 x 4 days | 100 | 5/5 | 5/5 | 0/5 |
| | 25 x 4 days | 100 | 0/5 | 0/5 | |
| **8c(M152)** | 100 x 4 days | 100 | 5/5 | 5/5 | 0/5 |
| | 50 x 4 days | 50 | 2/5 | 0/5 | 2/5 |
| **8d(M153)** | 100 x 4 days | 100 | 3/5 | 0/5 | 3/5 |
| **9a(M154)** | 100 x 4 days | 100 | 2/5 | 0/5 | 2/5 |
| **9c(M156)** | 100 x 4 days | 100 | 1/5 | 0/5 | 1/5 |
| **CQ** | 20 x 4 days | 99.0 | 5/5 | 0/5 | 5/5 |

711

712 *[a]Number of mice that survived untill day 28 post-infection/total number of mice in the group.*
713 *[b]Number of mice without parasitaemia (cured) through day 28 post-infection/total number of mice in*
714 *the group.*
715 *[c]p.o.,oral.*
716 *[d]Mice suvivng till day 28 were inoculated with 1x10[6] P yoelii parasitized erythrocytes to monitor*
717 *susceptibility to rechallenge.*
718

719 ***Table 3: Distribution pattern of 4-aminoquinoline derivatives in training and test sets***

| Dataset | Compounds | Activity ($pIC_{50}$) distribution | | | |
|---|---|---|---|---|---|
| | | *Min.* | *Max.* | *Avg.* | *SD* |
| **Training** | 111 | 5.30 | 8.33 | 6.85 | 0.87 |
| **Test set** | 57 | 5.30 | 8.48 | 6.84 | 0.86 |

720

721

722

723

724

725 ***Table 4: Binding scores (Total Score, Crash Score & Polar Score) of selected molecules***
726 ***from the in house database.***

| Cmpd.Code | Total Score | Crash Score | Polar |
|---|---|---|---|
| M32 | 1.1368 | -0.4986 | 1.4845 |
| M62 | 1.6703 | -0.8912 | 0.4415 |
| M64 | 1.6657 | -0.4918 | 1.4768 |
| M87 | 1.9119 | -0.9051 | 1.4469 |
| M96 | 4.2653 | -0.5227 | 1.4153 |
| M97 | 2.2337 | -0.5357 | 1.3241 |
| M100 | 2.8436 | -1.0254 | 0 |
| M113 | 2.3441 | -0.6026 | 1.4784 |
| M114 | 2.6098 | -0.7997 | 1.512 |
| M134 | 2.2171 | -0.6227 | 1.2771 |
| M158 | 3.1888 | -0.8168 | 2.0496 |
| M165 | 2.3102 | -0.9484 | 0 |

727

728 ***Table 5: Different types of non h-bond interactions between heme and CQ analogue***
729 ***(M96).***

| No. of non h-bond interactions | Distance (Å) | Category | Types |
|---|---|---|---|
| 1 | 3.39 | Electrostatic | Pi-Cation |
| 2 | 4.11 | Electrostatic | Pi-Anion |
| 3 | 4.72 | Hydrophobic | Pi-Pi Stacked |
| 4 | 5.00 | Hydrophobic | Pi-Alkyl |
| 5 | 3.78 | Hydrophobic | Pi-Alkyl |
| 6 | 4.32 | Hydrophobic | Pi-Alkyl |
| 7 | 4.32 | Hydrophobic | Pi-Alkyl |

730

731

732 ***Table 6: Goodness of fit of CoMFA and CoMSIA model for the antiplasmodial activities of***
733 ***chloroquine (CQ) analogues against 3D7 strain.***

| PLS Statistics | 3D7 | |
|---|---|---|
| | CoMFA Model | CoMSIA Model |
| $r^2$ nCV[a] | 0.924 | 0.885 |
| SEE[b] | 0.237 | 0.353 |
| Ftest[c] | 463.97 | 114.714 |
| $r^2$ CV[d] | 0.641 | 0.680 |
| SEP[e] | 0.596 | 0.574 |
| $r^2$ pred[f] | 0.656 | 0.608 |
| PLS components | 5 | 5 |
| Contribution | | |
| steric | 0.627 | 0.452 |
| electrostatic | 0.373 | 0.207 |
| hydrophobic | – | 0.341 |
| H-bond donor | - | - |
| H-bond acceptor | - | - |
| $r^2$ boot[g] | 0.946 | 0.933 |
| SEE boot[h] | 0.237 | 0.263 |
| $r^2$ LHO[i] | 0.479 | 0.535 |
| SD LHO[j] | 0.073 | 0.051 |
| $r^2$ 5cv[k] | 0.532 | 0.564 |
| SD 5cv[l] | 0.045 | 0.039 |

734 [a] *The predictable values correlation coefficient. For all models optimal number of PLS components are five.*
735 [b] *Standard error of estimate*
736 [c] *Ratio of $r^2$ explained to unexplained = $r^2/(1 - r^2)$*
737 [d] *Leave-one-out Predicted cross-validated correlation coefficient*

[e] *Standard error of prediction*
[f] *External predicted correlation coefficient for test set of compounds*
[g] *Average of correlation coefficient for 100 samplings using bootstrapped method*
[h] *Average standard error of estimate for 100 samplings using bootstrapped method*
[i] *Average cross-validated correlation coefficient for 50 runs using leave-half-out (LHO) group*
[j] *Standard deviation of average cross-validated correlation coefficient for 50 runs*
[k] *Average cross-validated correlation coefficient for 50 runs using five cross-validation group*
[l] *Standard deviation of average cross-validated correlation coefficient for 50 runs.*

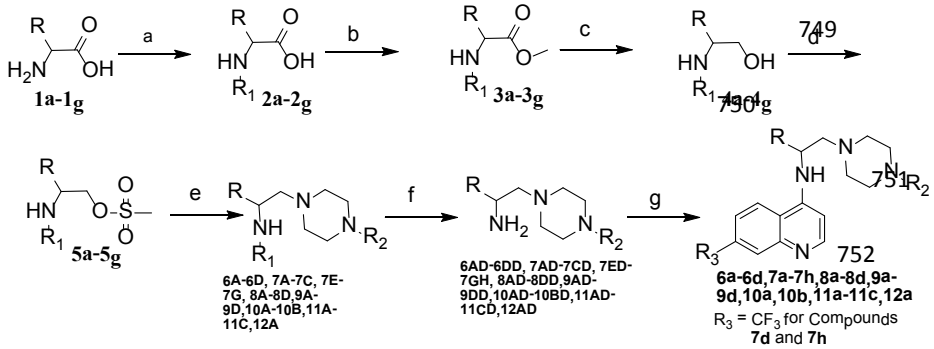


Where; R = H, $CH_3$, $CH_2CH(CH_3)_2$, CH $(CH_3)$ $C_2H_5$, $CH_2CH_2(S)$ $CH_3$, $CH_2$ $C_6H_5$, $CH_2$ indole;
$R_1$= Boc $R_3$ = Cl or $CF_3$

| Cmpd No | R | Cmpd No | R |
|---|---|---|---|
| 1a,2a,3a,4a,5a | H | 6a-6d | H |
| 1b,2b,3b,4b,5b | $CH_2CH(CH_3)_2$ | 7a-7h | $CH_2CH(CH_3)_2$ |
| 1c,2c,3c,4c,5c | $CH_2$ $C_6H_5$ | 8a-8d | $CH_2$ $C_6H_5$ |
| 1d,2d,3d,4d,5d | $CH_3$ | 9a-9d | $CH_3$ |
| 1e,2e,3e,4e,5e | $CH_2$-indole | 10a-10b | $CH_2$-indole |
| 1f,2f,3f,4f,5f | $CH_2CH_2(S)$ $CH_3$ | 11a-11c | $CH_2CH_2(S)$ $CH_3$ |
| 1g,2g,3g,4g,5g | CH $(CH_3)$ $C_2H_5$ | 12a | CH $(CH_3)$ $C_2H_5$ |

| Cmpd No | $R_2$ |
|---|---|
| 6a,7e | 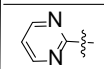 |
| 7b, 8b, 9c,10b, 11b |  |
| 7c, 7d,8c, 9b, 10a, 11c, 12a |  |
| 7a, 8a, 9d, 11a |  |
| 6b, 7f |  |
| 6d, 7g, 7h, 8d, 9a | 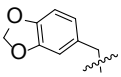 |
| 6c |  |

***Figure 1 Synthesis of compounds (6a-6d, 7a-7h, 8a-8d, 9a-9d, 10a, 10b, 11a-11c and 12a); Reagents and Conditions:*** *(a) $(Boc)_2O$, NaOH/Dioxane, 0°C, 2-3 h; (b) $K_2CO_3$, DMF, MeI, 0°C, 6-8h;(c) $NaBH_4$, MeOH, THF, 65°C, 1h; (d) Triethyl amine, Methane sulphonyl chloride, THF, 0 °C, 45 min; (e) N-Substituted piperazines, Triethyl amine, acetonitrile, $N_2$ atm, r.t, 40 h; (f) 20% HCl/dioxane 1h; (g) 4,7-dichloroquinoline, and/or 4-chloro-7-(trifluoromethyl)quinoline, Phenol, 160°C, 4-6 h.*

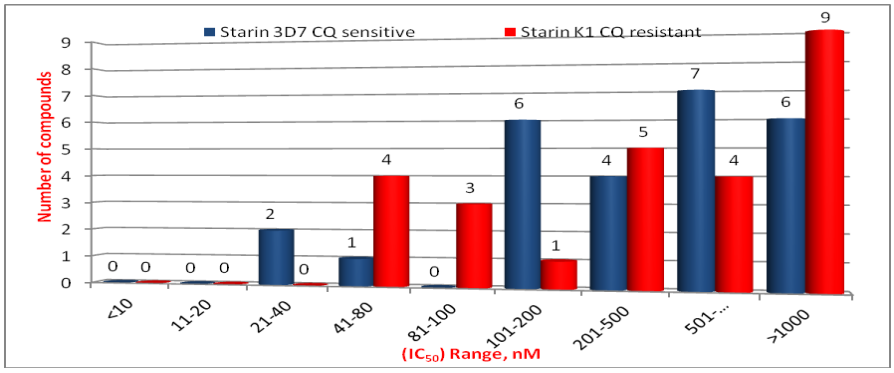


***Figure 2:*** Histogram showing the number of compounds evaluated against P. falciparum in the present study.

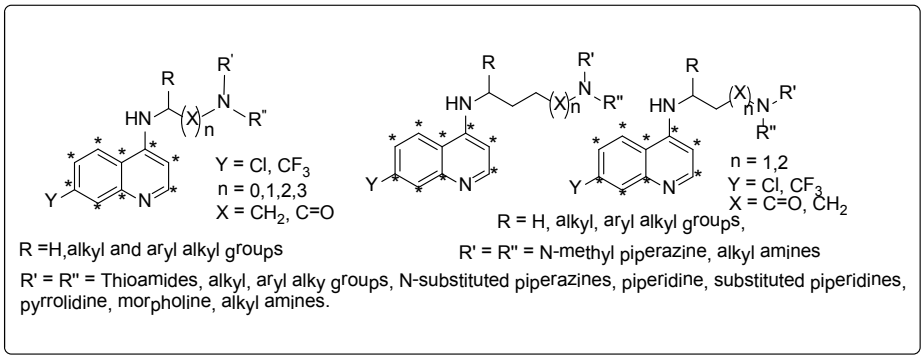


***Figure 3:*** General structures of the all synthesized compounds. The asterisk marked the atoms which are common to all structures and used for the CoMFA/CoMSIA alignment.

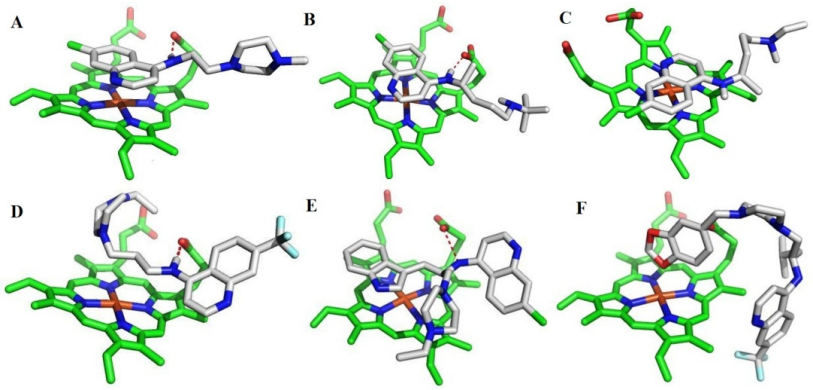


***Figure 4:*** Molecular docking of most active ('A': M96, 'B': M64 and 'C': M62) and less active ('D': M32, 'E': M158 and 'F': M165) compounds with heme. Red colour (---) indicate h-bond interaction.

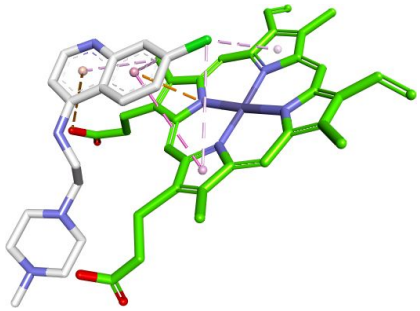

***Figure 5:*** Non h-bond interactions between heme and M96. Yellow colour (---) indicate electrostatic interactions whereas pink colours (---) indicate hydrophobic interactions.

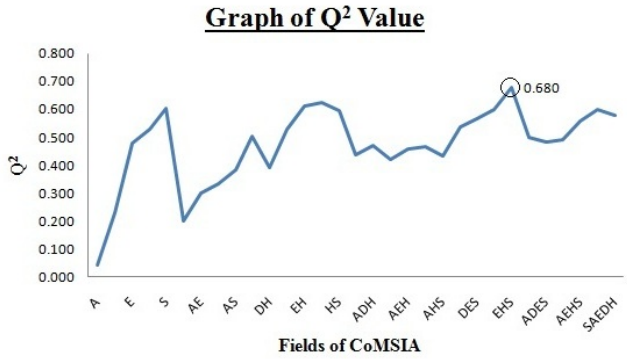


***Figure 6:*** A graphical Plots of $Q^2$ values of CoMSIA models which indicated single as well as multiple field combinations for CQ analogues as antiplasmodial inhibitors against the 3D7 strain. In this plot, x-axis indicate the fields of CoMSIA with single letters i.e. A (HB-Acceptor), D (HB-donor), E (electrostatic), H (hydrophobic) and S (steric). The field combinations which led to the model with ideal $Q^2$ (y-axis) is marked with circle.

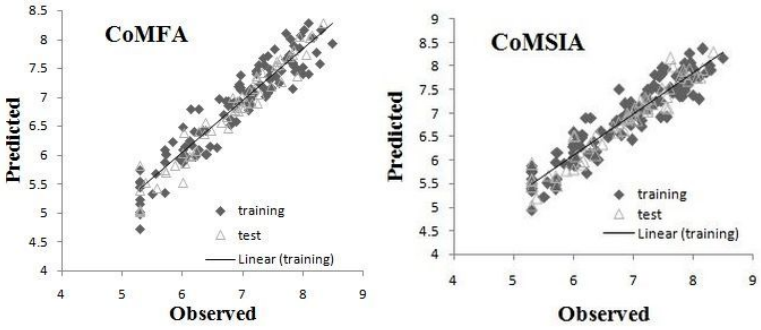


***Figure 7:*** The scatter plots of experimental $pIC_{50}$ values versus predicted $pIC_{50}$ values derived from CoMFA/CoMSIA training (filled box) and the test set (triangle) of CQ derivatives for Plasmodium falciparum 3D7 strain.

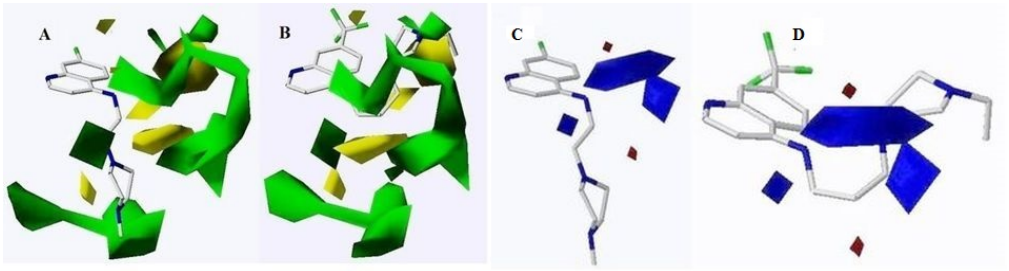


***Figure 8:*** Two different contour maps including Steric field contour maps (**A&B**), & electrostatic field contour maps(**C&D**) of CoMFA 3D-QSAR are appeared for CQ analogues as antiplasmodial inhibitors against 3D7 strain. In this figure, the poses of compounds **M96 (active)** & **M32 (inactive)** are used to demonstrate the contour maps. Colour code specified favourable & unfavourable regions. Here, green contours indicate sterically favourable regions and yellow contours shows sterically unfavourable regions for the biological activity (A&**B**). Again, blue contours indicate electropositive regions & red contours pointed out the electronegative regions (**C&D**).

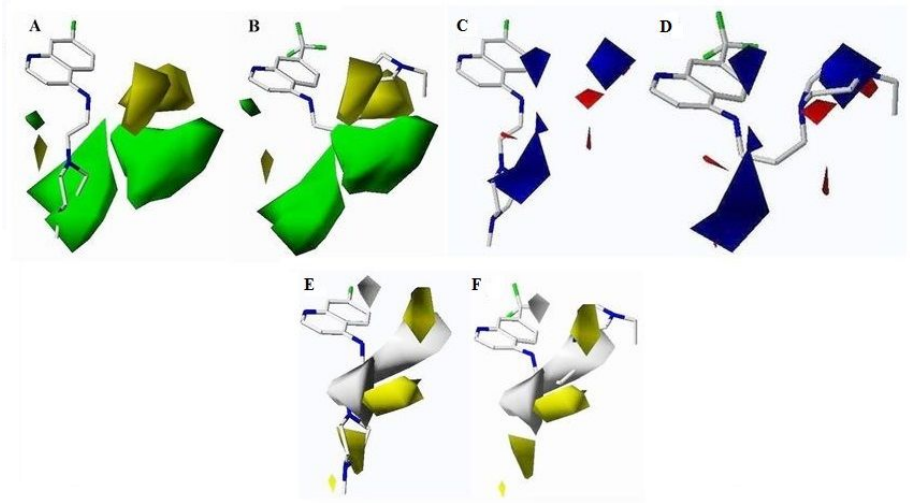


***Figure 9:*** Three different contour maps including Steric field contour maps (**A&B**), electrostatic field contour maps(**C&D**) and hydrophobic contour maps (**E&F**) of CoMSIA 3D-QSAR are appeared for CQ analogues as antiplasmodial inhibitors against 3D7 strain. In this figure, the poses of compounds **M96 (active)** & **M32 (inactive)** are used to demonstrate the contour maps. Colour code specified favourable & unfavourable regions. Here, green contours indicate sterically favourable regions and yellow contours shows sterically unfavourable regions for the biological activity (A&**B**). Similarly, blue contours indicate electropositive regions & red contours pointed out the electronegative regions (**C&D**). Again, yellow contours designate hydrophobic favourable regions whereas white contours indicate hydrophobic unfavourable regions for the activity (**E&F**).